MOLECULAR AND CELLULAR BIOLOGY, Mar. 2009, p. 1176–1188 Vol. 29, No. 5
0270-7306/09/$08.00+0 doi:10.1128/MCB.01599-08

The Double-Histone-Acetyltransferase Complex ATAC Is Essential for Mammalian Development▽

Sebastián Guelman,[1] Kenji Kozuka,[1] Yifan Mao,[1] Victoria Pham,[2] Mark J. Solloway,[3] John Wang,[1] Jiansheng Wu,[2] Jennie R. Lill,[2] and Jiping Zha[1]*

Department of Pathology, Genentech Inc., South San Francisco, California[1]; Department of Protein Chemistry, Genentech Inc., South San Francisco, California[2]; and Department of Molecular Biology, Genentech Inc., South San Francisco, California[3]

Received 12 October 2008/Returned for modification 3 November 2008/Accepted 9 December 2008

Acetylation of the histone tails, catalyzed by histone acetyltransferases (HATs), is a well-studied process that contributes to transcriptionally active chromatin states. Here we report the characterization of a novel mammalian HAT complex, which contains the two acetyltransferases GCN5 and ATAC2 as well as other proteins linked to chromatin metabolism. This multisubunit complex has a similar but distinct subunit composition to that of the *Drosophila* ADA2A-containing complex (ATAC). Recombinant ATAC2 has a weak HAT activity directed to histone H4. Moreover, depletion of ATAC2 results in the disassembly of the complex, indicating that ATAC2 not only carries out an enzymatic function but also plays an architectural role in the stability of mammalian ATAC. By targeted disruption of the *Atac2* locus in mice, we demonstrate for the first time the essential role of the ATAC complex in mammalian development, histone acetylation, cell cycle progression, and prevention of apoptosis during embryogenesis.

Chromatin is a dynamic nucleoprotein filament that undergoes dynamic chemical and conformational changes throughout the eukaryotic cell cycle (3). The compaction state of chromatin has a direct impact on transcription, replication, and DNA repair and recombination, all of which are nuclear processes that require DNA as a template. Successful execution of these processes requires modification of the nucleosome architecture by a variety of cellular machineries, which include chromatin-remodeling complexes as well as enzymatic complexes involved in posttranslational modifications of the histone tails (26, 50).

Histone acetyltransferases (HATs) are the key enzymes responsible for the acetylation of the histone tails. One of the most-studied HATs is GCN5, a protein conserved from *Saccharomyces cerevisiae* to humans (9, 51). This protein carries two conserved domains: an acetyltransferase domain required for its catalytic activity and a bromodomain that binds acetylated lysine residues (8, 40, 41). Recombinant yeast Gcn5 preferentially modifies histone H3 K14 and histone H4 K8 and K16 (28). However, the incorporation of yeast Gcn5 into native multisubunit complexes expands its substrate specificity, enabling it to acetylate histone H3 K9 and K18 in addition to K14 (19). In vivo studies of metazoans show a similar yet not identical substrate specificity for GCN5. For instance, polytene chromosomes isolated from *gcn5* mutant fly larvae show reduced levels of acetylated H3 K9 and K14, as well as H4 K5 and K12 (10, 12). In addition, chicken DT40 cells devoid of GCN5 selectively display reduced levels of acetylated histone H3 K9 (25).

To date, mammalian GCN5 has been identified in SPT3-TAF9-GCN5 acetyltransferase (STAGA) and the TATA-binding protein (TBP)-free TAF complex (TFTC), two multisubunit complexes that facilitate transcription from chromatin templates by acetylating histones H3 and H4 (7, 32, 33). These two highly similar complexes contain a subset of the TBP-associated factors (TAFs) found in TFIID as well as orthologues of the yeast SAGA subunits Ada1, Ada2, Ada3, Spt3, Spt7, Sgf29, and Tra1 (7, 11, 32, 33). Additional subunits of STAGA/TFTC include Ataxin-7, the splicing factor SAP130, and the deubiquitinating enzyme USP22 (6, 23, 33, 63, 64). Recently, a very distinct GCN5-containing complex, the ADA2A-containing complex (ATAC), was purified and characterized from *Drosophila* cells (21, 49).

In the present study, we report the first biochemical and functional characterization of mammalian ATAC2, which has a conserved GCN5 *N*-acetyltransferase domain and is the orthologue of the recently characterized *Drosophila* ATAC2 (37, 49). Mammalian ATAC2 was originally identified in a yeast two-hybrid assay as a binding partner of the cysteine- and glycine-rich protein 2 (CRP2) and was therefore named CRP2 binding partner (53). However, the functions of ATAC2 in mammalian cells are otherwise unknown. To gain mechanistic insight into ATAC2 function, we affinity purified the ATAC2-containing complex and discovered the evolutionarily conserved mammalian ATAC, which includes GCN5 and other proteins linked to chromatin metabolism and has a similar but not identical subunit composition to that of a recently characterized human ATAC (52). While ATAC2 has weak HAT activity in vitro, it plays a crucial role in maintaining the structural integrity of ATAC. We generated *Atac2*-null mice to dissect its function in vivo. Homozygous knockout (KO) animals die during early embryogenesis, with severe growth retardation, increased apoptosis, and alterations in the cell cycle. Embryos deficient in *Atac2* and cell lines in which ATAC2 is depleted display reduced levels of acetylated histones H3 and H4 at specific lysines. Overall, our work reveals that ATAC2 is

* Corresponding author. Mailing address: Department of Pathology, Genentech Inc., 1 DNA Way MS 72B, South San Francisco, CA 94080. Phone: (650) 225-4947. Fax: (650) 225-8989. E-mail: zha.jiping@gene.com.

▽ Published ahead of print on 22 December 2008.

an architectural and catalytic protein of the novel mammalian ATAC that is crucial for embryonic viability and cell cycle progression.

MATERIALS AND METHODS

Expression and purification of recombinant proteins. A cDNA fragment coding for amino acids 603 to 782 of ATAC2 and the full-length cDNA for *Gcn5* were inserted into pET16b (Novagen) for expression in BL21(DE3) bacteria. The full-length sequence for *Atac2* was cloned into pAcHLT-A (BD Biosciences) for expression in Sf9 cells. The resulting His-tagged fusion proteins were purified over Ni-nitrilotriacetic acid agarose (Qiagen) according to the manufacturer's instructions, with an extra 40 mM imidazole wash step to remove nonspecific proteins.

Generation of polyclonal antibodies. Rabbits were immunized with a recombinant C-terminal fragment of ATAC2 (amino acids 603 to 782) (Invitrogen). Antibodies directed to YEATS2 were obtained by immunizing rabbits with the peptide CPPDKREENDQSTHK conjugated to keyhole limpet hemocyanin (Yenzym).

Generation of stable cell lines. The cDNAs for human *Atac2* (GenBank accession no. NM_020536), *Gcn5*, *Mbip*, *Wdr5*, and *Ada1*/*Staf42* were inserted into pcDNA5/FRT (Invitrogen). All of these constructs were fused to a C-terminal tag consisting of two hemagglutinin (HA) epitopes followed by two FLAG sequences. The pcDNA5/FRT-derived constructs were cotransfected with pOG44 into Flp-in 293 cells according to the manufacturer's instructions (Invitrogen). Stable cell lines were selected in the presence of 0.2 μg/ml hygromycin.

The cDNA for human *Atac2* fused to two HA and two FLAG tags was inserted into pMSCVpuro (Clonetech). Retroviral transduction was carried out to infect mouse C2C12 cells. Stable cell lines were selected with 2 μg/ml puromycin.

Affinity purification. Nuclear extracts were prepared from Flp-in 293, ATAC2-FLAG Flp-in 293, MBIP-FLAG Flp-in 293, C2C12, and ATAC2-FLAG C2C12 cells, using a standard protocol (1). Approximately 10 mg of nuclear extract was incubated with 150 μl M2-agarose beads (Sigma) overnight at 4°C. The beads were washed four times with 300 mM wash buffer (10 mM HEPES, pH 7.9, 25% glycerol, 1.5 mM $MgCl_2$, 300 mM KCl, 0.1% Triton X-100), followed by two washes with 100 mM wash buffer (10 mM HEPES, pH 7.9, 25% glycerol, 1.5 mM $MgCl_2$, 100 mM KCl, 0.1% Triton X-100). Elution was achieved by two consecutive room temperature incubations of the beads with 0.5 mg/ml triple-FLAG peptide (Sigma) in 200 μl of 100 mM wash buffer. All buffers contained phenylmethylsulfonyl fluoride and protease inhibitor cocktail (Roche). A 10% volume of each elution was analyzed by sodium dodecyl sulfate-polyacrylamide gel electrophoresis (SDS-PAGE) and silver staining. The remainders of the two eluates were pooled, concentrated, and prepared for mass spectrometry (MS).

MS and bioinformatic analysis. Samples were reduced in SDS sample buffer, alkylated with iodoacetamide, and separated by SDS-PAGE. After Coomassie blue staining and destaining of the gel, 20 to 30 bands were excised from the gel, diced into smaller pieces, washed, and digested overnight at 37°C with 1 μg of trypsin (Promega). The reactions were quenched, and the samples were concentrated and subjected to MS analysis.

Samples were injected via an autosampler for separation by reverse phase chromatography on a NanoAcquity UPLC system (Waters). Peptides were loaded onto a precolumn (5-μm Symmetry C_{18} column) and separated using an analytical column (1.7-μm BEH-130 C_{18} column). Peptides were eluted directly into a nanospray ionization source and analyzed using an LTQ XL-Orbitrap mass spectrometer (Thermo Fisher). Precursor ions were analyzed in an FTMS instrument at 60,000 resolution. MS/MS was performed in an LTQ instrument operated in data-dependent mode, whereby the top 5/10 most abundant ions were subjected for fragmentation. Data were searched using the Mascot search algorithm (Matrix Sciences), and Mascot output files were uploaded into Scaffold (Proteome Software).

Gel filtration chromatography. Affinity-purified ATAC, isolated from MBIP-FLAG Flp-in 293 cells, or 2 mg of nuclear extract from HEK293 cells was applied to a Superose 6 10/300GL column (GE Healthcare). High-molecular-weight standards (GE Healthcare) were separated under the same conditions. The buffer composition was 20 mM HEPES, pH 7.6, 10% glycerol, 300 mM KCl, 0.2 mM EDTA, 0.1% Triton X-100, and protease inhibitors. Even fractions were analyzed by Western blotting using commercially available antibodies against GCN5 (Biolegend), ADA3 (Abcam), ADA2b (Abnova), WDR5 (Millipore), ADA2a, DR1, MBIP, and TAF12 (Proteintech) and the antibodies that we developed against ATAC2 and YEATS2.

HAT assays. Recombinant proteins or purified complexes were incubated for 1 h at 37°C with 2 μg core histones (Millipore) and 0.5 μCi of [^{3}H]acetyl coenzyme A in a 50-μl reaction volume. Histone acetylation was detected by fluorography (16).

siRNA knockdowns and coimmunoprecipitations. The sequences in *Atac2*, *Mbip*, and *Gcn5* targeted by small interfering RNA (siRNA) oligonucleotides were CGACGCACCTCTCGATTAC, GAGATGATGTGGTGAAAAT, and GCGCATGCCTAAGGAGTAT, respectively. Nontargeting siRNA was purchased from Dharmacon. HEK293 cells were transfected in 60-mm dishes, using Dharmafect I, according to a protocol established by Dharmacon. After 72 h, small-scale nuclear extracts were prepared using an NE-PER nuclear extraction kit (Pierce) to detect the levels of protein depletion by Western blotting. Alternatively, cells were lysed in 50 mM Tris, pH 7.5, 0.5% NP-40, 300 mM NaCl, 1 mM EDTA, 10% glycerol, and protease inhibitors. Coimmunoprecipitations were performed using anti-GCN5 or anti-WDR5 antibodies and 1 mg of whole-cell extract. Protein A/G beads (Pierce) were used to bring down the immunoprecipitated material. The beads were washed four times in lysis buffer, denatured, and analyzed by Western blotting.

Generation of inducible shRNA knockdown cell lines. A double-stranded hairpin oligonucleotide targeting the sequence CGACGCACCTCTCGATTAC of *Atac2* was inserted into pHUSH (20). Retrovirus transduction was used to introduce the vector carrying the *Atac2* short hairpin RNA (shRNA) cassette into A549 and HEK293 cells, which were selected in puromycin at 2 and 6 μg/ml, respectively. Individual clones were isolated and screened for protein depletion by immunoprecipitation with ATAC2 antibodies, followed by anti-ATAC2 Western blotting. Induction of the knockdown was achieved by a 6-day treatment with 1 μg/ml doxycycline.

Analysis of histone acetylation. Individual embryonic day 8.5 (E8.5) embryos were homogenized in 50 to 100 μl of RIPA buffer. Two micrograms of extract was analyzed by Western blotting, using the following antibodies from Millipore: anti-acetylated H3 on lysine 9 (H3 ac K9), anti-acetylated H3 on lysine 14 (H3 ac K14), anti-acetylated H4 on lysine 5 (H4 ac K5), anti-acetylated H4 on lysine 8 (H4 ac K8), anti-acetylated H4 on lysine 12 (H4 ac K12), and anti-acetylated H4 on lysine 16 (H4 ac K16). Anti-H3 (Abcam) served as the loading control. Western blot images were captured on a Fujifilm LAS-3000 instrument, and bands were quantified using Image Reader software (Fuji). The intensity of each acetyl-K band was normalized to the total amount of histone H3, and the normalized mean for wild-type (WT) embryos was arbitrarily set to 1. A two-tailed *t* test was used to compare WT and KO groups. Differences were considered significant for *P* values of <0.05. Histones were enriched by acid extraction from *Atac2* shRNA stable cell lines grown in the presence or absence of doxycycline. One microgram of acid-extracted proteins from HEK293 cells or 5 μg of proteins from A549 cells was analyzed by Western blotting, followed by quantification and *t* test analysis.

Cell cycle analysis. Individual cells were collected by dissociating E9.5 embryos in Dulbecco's modified Eagle's medium containing 0.8 mg/ml collagenase-dispase (Roche) for 1.5 h at 37°C. A549 stable cell lines carrying the *Atac2* shRNA construct were grown for 6 days in the presence or absence of doxycycline. Cells were washed twice in phosphate-buffered saline (PBS) and resuspended in 0.1% sodium citrate, 0.3% NP-40, 50 μg/ml propidium iodide (PI), and 20 μg/ml RNase A. DNA contents were assayed by flow cytometry. Data were analyzed using ModFit software.

PI exclusion assay. A549 *Atac2* shRNA cells were grown for 6 days in the presence or absence of doxycycline, harvested by trypsinization, washed with PBS, incubated with 1 μg/ml PI, and analyzed by fluorescence-activated cell sorting (FACS).

Generation of *Atac2*-deficient mice. Embryonic stem (ES) cells with the retroviral gene trap vector VICTR48 inserted into the *Atac2* locus were generated. The KO mice were produced in a collaboration between Genentech and Lexicon Pharmaceuticals to analyze the functions of about 500 secreted and transmembrane proteins. Methods for gene trapping in ES cells and characterization of retroviral gene trap vector insertion points have been described previously (59, 60). *Atac2*-targeted ES cells were microinjected into blastocysts and implanted into C57BL/6 female mice. Heterozygous mice were further backcrossed onto the C57BL/6 background.

Genotyping. Yolk sacs from E8.5 to E11.5 embryos were digested for 5 hours in 30 μl of 10 mM Tris, pH 8.3, 50 mM KCl, 2.5 mM $MgCl_2$, 0.1 mg/ml gelatin, 0.45% NP-40, 0.45% Tween 20, and 0.7 mg/ml proteinase K. PCRs were carried out using three primers, one of which amplifies both the WT and the KO alleles, while the other two are specific to each of the alleles (shown in Fig. 4). The DNA sequences of the primers are as follows: GGAAATGGAGACAGAATGTGTG, ATAAACCCTCTTGCAGTTGCATC, and CTATCTGAGCCGGGCGTGGT AGTGCC. To obtain DNAs from fixed paraffin-embedded slides, tissue was scraped off and DNAs were isolated with a Picopure DNA extraction kit (Arc-

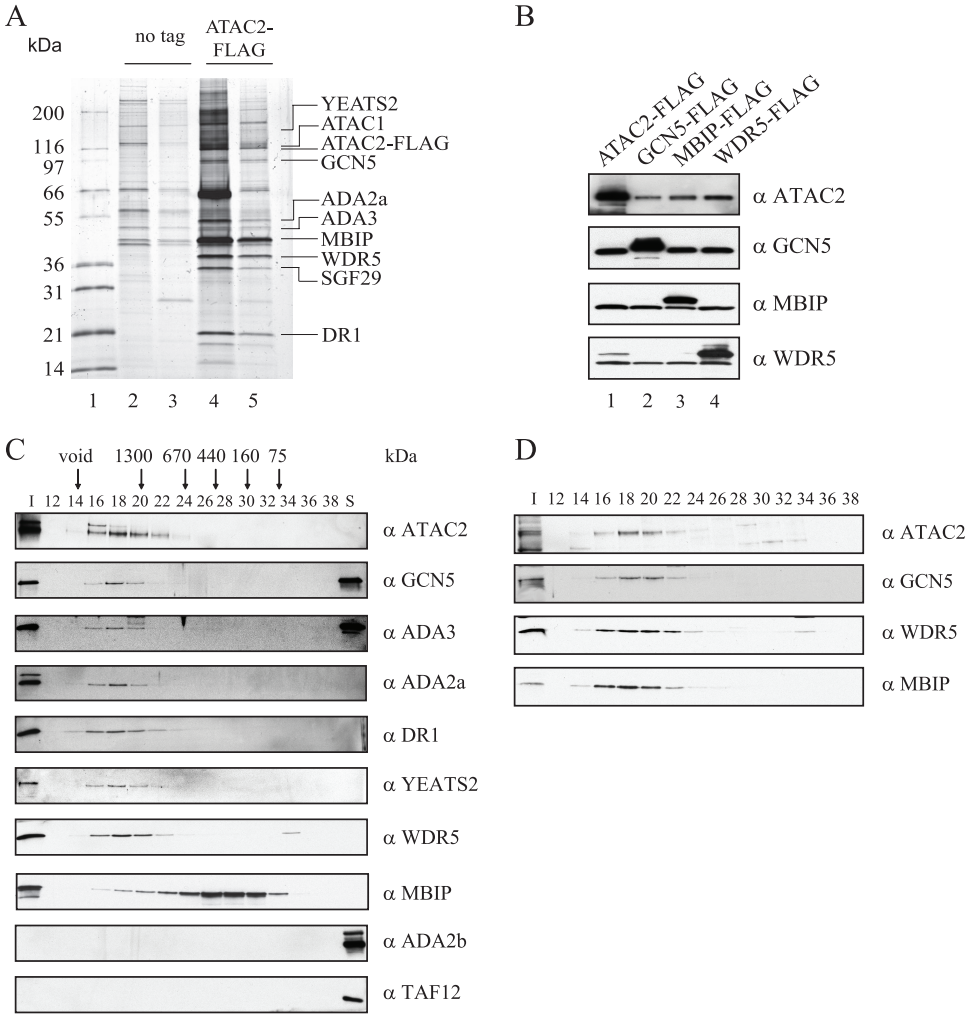

FIG. 1. Purification of mammalian ATAC2-containing complex from HEK293 cells. (A) Purified complexes from HEK293 cells expressing ATAC2-FLAG were analyzed by SDS-PAGE and silver staining. Lane 1, molecular size standards; lanes 2 and 3, consecutive eluates from HEK293 cells (no tag); lanes 4 and 5, consecutive eluates from ATAC2-FLAG cells. The proteins identified by MS are indicated. (B) Extracts from HEK293 cells expressing FLAG-tagged ATAC2, MBIP, GCN5, or WDR5 were immunoprecipitated with anti-FLAG antibodies, and the immunoprecipitated material was analyzed by Western blotting. (C) Mammalian ATAC was applied to a Superose 6 column. Even fractions were analyzed by Western blotting, using antibodies against ATAC2, GCN5, ADA3, ADA2a, DR1, WDR5, YEATS2, MBIP, ADA2b, and TAF12. Lane I, input (affinity-purified ATAC); lane S, affinity-purified STAGA. (D) Nuclear extract from HEK293 cells was applied to a Superose 6 column. Even fractions were analyzed by Western blotting. Lane I, input.

turus). To genotype mouse tails, DNAs were extracted using an Extract-N-Amp kit (Sigma).

Whole-mount RNA in situ hybridization. In situ hybridization was performed as described previously (47). The following mouse cDNAs, purchased from Open Biosystems, were used as templates to prepare the riboprobes: *Atac2*, *Dll1*, *Mlc2v*, *Fgf8*, *Twist1*, *Tcf15*, *Wnt1*, *Pax3*, and *Foxa2*.

Histological studies. Deciduae corresponding to E8.5 embryos were fixed in 10% formalin overnight at 4°C, dehydrated, and embedded in paraffin. Five-micrometer-thick sagittal sections were prepared and stained with hematoxylin and eosin. Immunohistochemistry was carried out using antibodies against cleaved caspase-3 (Cell Signaling Technology) according to the manufacturer's procedures. Hematoxylin was used as a counterstain.

RESULTS

ATAC2 associates with GCN5 and other proteins linked to chromatin metabolism. *Drosophila* ATAC (dATAC) carries GCN5 and ATAC2, two proteins with acetyltransferase activity (49). We identified a human protein with a C terminus (amino acids 463 to 782) 45% identical to that of fly ATAC2, which suggests that the ATAC complex is likely to be present in mammals. We reasoned that biochemical characterization of the putative mammalian ATAC would allow us to compare the similarities and differences of its functions across species. Overexpressed and tagged ATAC2 was utilized to facilitate the purification and MS analysis of its associating proteins in human HEK293 and mouse C2C12 cells, which were chosen based on their high endogenous levels of *Atac2* mRNA. ATAC2 tagged with FLAG at the C terminus, as well as its interacting proteins, was affinity purified and analyzed by electrophoresis followed by silver staining (Fig. 1A). Several bands were present in purified material from ATAC2-FLAG-expressing cells but not in

TABLE 1. Proteins identified by mass spectrometry

Protein	ATAC2-FLAG HEK293 cells		ATAC2-FLAG C2C12 cells		MBIP-FLAG HEK293 cells	
	No. of unique peptides	% Coverage	No. of unique peptides	% Coverage	No. of unique peptides	% Coverage
ATAC2	21	30	19	25	22	26
GCN5	10	8	4	5	17	22
ADA2a	14	35	5	15	11	22
ADA3	8	27	7	20	9	24
ZZZ3/ATAC1	26	32	24	34	35	43
MBIP	16	46	12	37	23	51
WDR5	8	36	5	21	9	28
YEATS2	53	48	39	35	72	62
SGF29	5	23	6	26	7	23
DR1	2	12	2	12	4	20

that from parental cells. MS analysis of ATAC2-FLAG cells revealed nine proteins that are homologous to the subunits of the recently reported ATAC in *Drosophila melanogaster* (Table 1). The sequence coverage of ATAC2 by MS analysis was 30% and 25% for the human (HEK293) and mouse (C2C12) cell lines, respectively. GCN5, ADA3, and SGF29, which were previously identified in STAGA and TFTC (6, 11, 33), were also found in the mammalian ATAC. In addition, seven ATAC-specific components were discovered, including ADA2a, ZZZ3, mitogen-activated protein kinase (MAPK) upstream kinase-binding inhibitory protein (MBIP), WDR5, YEATS2, and DR1 (21, 49). MBIP, a leucine zipper-like motif-containing protein originally identified as an inhibitor of the MAPK upstream kinase, appears to be the only mammal-specific component (17). Some of the proteins in ATAC are also present in other chromatin-modifying complexes. For instance, the WD40 repeat protein WDR5 is found in the mammalian Set1-like histone methyltransferase complexes (14, 58). YEATS2 has a conserved YEATS (Ynl107, ENL, AF9, and TFIIF small subunit) domain, which is present in a small number of proteins that are subunits of chromatin-modifying complexes, including the HATs SAS and NuA4/TIP60, and chromatin-remodeling complexes, such as SWI/SNF (15, 38, 46, 61). Lastly, the TBP-binding protein DR1 was also present in the purified complex (24, 27, 34, 54, 57). DR1 usually associates with DRAP1 through histone fold motifs to form the NC2 complex, which negatively regulates transcription initiation (18). However, DRAP1 was not detected by MS analysis in our purified preparations, suggesting a novel function for DR1. These MS hits were further confirmed using a separate preparation of complex purified from HEK293 cells expressing MBIP-FLAG, which yielded peptides for the same proteins as those identified by the ATAC2-FLAG purification (Table 1). None of these subunits, except for four peptides for WDR5 in the mock HEK293 purification, were detected in purifications from parental HEK293 or C2C12 cells, indicating that our experiments accurately identified a mammalian ATAC.

The MS results were corroborated by anti-FLAG coimmunoprecipitation with cells expressing FLAG-tagged ATAC2, MBIP, GCN5, and WDR5. We confirmed that MBIP, GCN5, and WDR5 interact with ATAC2 as well as with each other (Fig. 1B). In addition, coimmunoprecipitation was performed with endogenous proteins in HEK293, A549, and C2C12 cells. Anti-WDR5 antibody brought down WDR5 as well as GCN5, ATAC2, MBIP, and DR1 (Fig. 2C, lane 5, and D, lanes 3 and 7), ruling out the possibility that these interactions were due to overexpressed tagged proteins. Because coimmunoprecipitation does not address whether these proteins are assembled in a multisubunit complex, we applied the affinity-purified complex isolated from the HEK293 cells expressing MBIP-FLAG to a Superose 6 gel filtration column and analyzed the elution patterns of the different proteins by Western blotting. We focused our efforts on ATAC2, GCN5, ADA3, ADA2a, WDR5, YEATS2, and DR1 because specific antibodies were available (Fig. 1C). These seven proteins eluted in the same fractions (fractions 16 to 20) of the column, with an approximate molecular size range of 1.5 MDa. This mammalian ATAC is distinct from previously characterized GCN5-containing complexes because ADA2b and TAF12, which are two subunits of STAGA/TFTC, were absent from the MBIP immunoprecipitates (Fig. 1C, lane 1). Conversely, purified STAGA did not contain ADA2a, WDR5, YEATS2, DR1, or MBIP (Fig. 1C, right lane). The tagged MBIP eluted in fractions 16 to 20 but peaked in the lower-molecular-weight range. To determine whether this broad elution pattern was due to overexpression, which might alter how MBIP is assembled normally, we examined the endogenous complex in HEK293 cells. Unlike the overexpressed protein, endogenous MBIP comigrated with ATAC2, GCN5, and WDR5 by gel filtration (Fig. 1D). The elution pattern of the endogenous ATAC was identical to that of the complex purified from MBIP-FLAG cells. Taken together, our experiments uncovered an evolutionarily conserved mammalian ATAC which is biochemically distinct from STAGA and TFTC.

Mammalian ATAC is a HAT that acetylates histones H3 and H4. dATAC is a potent HAT with two acetyltransferases, namely, GCN5 and ATAC2 (49). Similarly, our affinity-purified mammalian ATAC displayed robust in vitro HAT activity on histones H3 and H4, which increased proportionally to the amount of complex used in the assay (Fig. 2B, lanes 1 to 3). A similar profile of HAT activity was also observed when ATAC was purified from cells expressing ATAC2-FLAG, MBIP-FLAG, or WDR5-FLAG, confirming that a carboxy-terminal tag on any of these subunits does not interfere with the catalytic activity of the complex (data not shown). To establish the respective contributions of ATAC2 and GCN5 to the overall activity of ATAC, we first determined the approximate levels of GCN5 and ATAC2 within ATAC by comparing them to known amounts of recombinant proteins (Fig. 2A). Based on these quantifications, we performed HAT assays using amounts of recombinant His-tagged GCN5 and ATAC2 comparable to those in the purified complex. We observed that GCN5 was as robust as the ATAC in acetylating histone H3 but not H4 (Fig. 2B, compare lanes 1 to 3 to lanes 4 to 6). In contrast, comparable amounts of ATAC2 did not exhibit any significant HAT activity (data not shown); however, a 10-fold increase in recombinant ATAC2 had weak HAT activity, with a preference for H4 (Fig. 2B, lanes 7 to 9). These data suggest that ATAC2 and/or GCN5 may require other proteins in the complex to potentiate catalytic activity toward H4. In fact, Ada2, a subunit of yeast SAGA, strongly enhances the catalytic activity of recombinant Gcn5 on core histones (2). Furthermore, ATAC2 may have additional roles in ATAC besides its weak catalytic function.

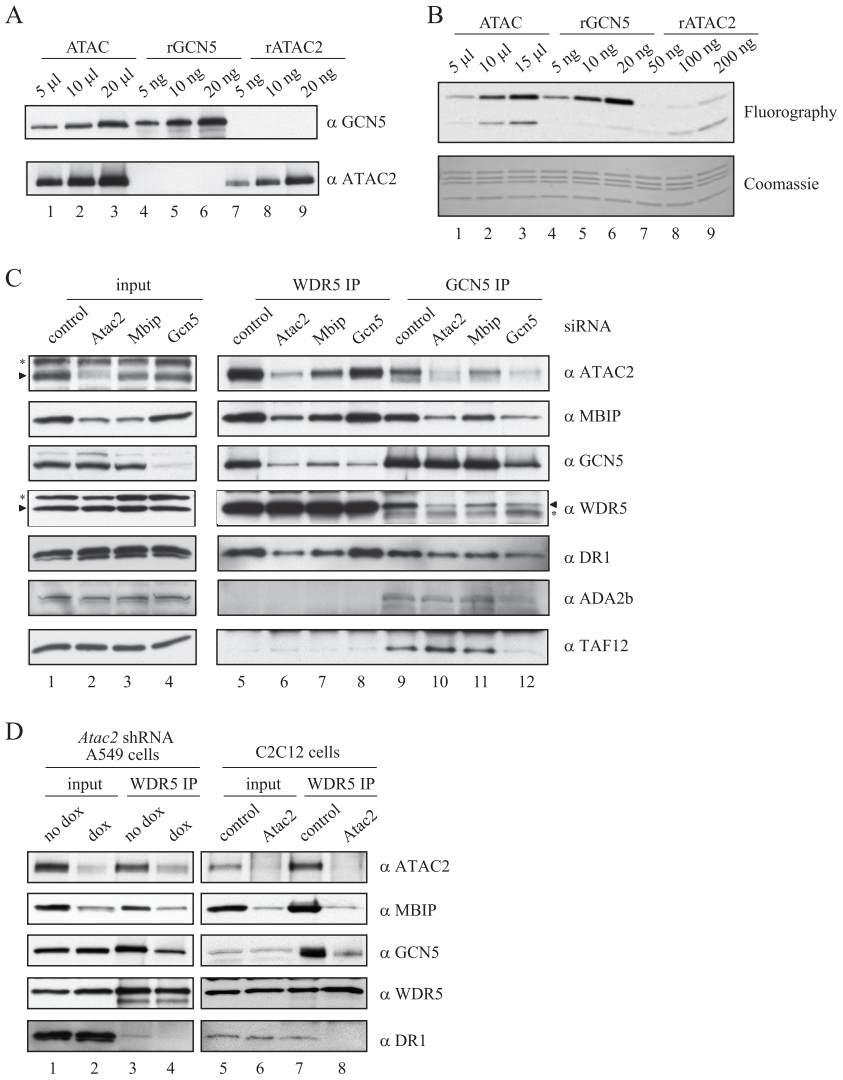

FIG. 2. ATAC2 acetylates H4 and stabilizes the integrity of ATAC. (A) Western blotting to determine the amounts of ATAC2 and GCN5 present in purified ATAC. Lanes 1 to 3, 5, 10, and 20 μl ATAC purified from HEK293 cells expressing MBIP-FLAG; lanes 4 to 6: 5, 10, and 20 ng recombinant His-GCN5; lanes 7 to 9, 5, 10, and 20 ng recombinant His-ATAC2. (B) HAT assays were carried out using increasing amounts of ATAC (5, 10, and 15 μl; lanes 1 to 3), His-GCN5 (5, 10, and 20 ng; lanes 4 to 6), and His-ATAC2 (50, 100, and 200 ng; lanes 7 to 9). The bottom panel is a Coomassie gel that shows the loading of the four core histones. The top panel is a fluorograph of the same gel to detect ^{3}H-labeled acetylated histones. (C) HEK293 cells were transfected with siRNAs for *Atac2*, *Mbip*, and *Gcn5* or with a nontargeting siRNA (control). Extracts (lanes 1 to 4) were immunoprecipitated with antibodies to WDR5 (lanes 5 to 8) or GCN5 (lanes 9 to 12), and the immunoprecipitated material was analyzed by Western blotting. Arrowheads point to specific bands. Cross-reacting bands are shown with asterisks. (D) An A549 stable cell line expressing doxycycline-inducible *Atac2* shRNA was grown for 3 days in the absence or presence of doxycycline (no dox and dox lanes, respectively). C2C12 cells were transfected for 3 days with a siRNA oligonucleotide that targets mouse *Atac2* or a nontargeting control siRNA. Nuclear extracts (input) were prepared from A549 and C2C12 cells. Whole-cell extracts were immunoprecipitated with antibodies against WDR5, and the immune complexes (WDR IP) were analyzed by Western blotting.

ATAC2 and MBIP are required for the structural integrity of mammalian ATAC. Proteins can be stabilized by protein-protein interactions in a multisubunit complex, as demonstrated for specific subunits of the STAGA and COP9 signalosome complexes (30, 44). We investigated whether ATAC2 can contribute to the stability of other ATAC subunits by using a loss-of-function approach. ATAC2 was efficiently depleted by siRNA knockdown in HEK293 cells (Fig. 2C, lane 2). Concomitant with ATAC2 depletion, the MBIP level was also decreased (lane 2 in the MBIP blot). A reciprocal yet more modest effect was observed on ATAC2 stability when MBIP was depleted (compare lanes 1 and 3 in the ATAC2 blot). These data suggest that ATAC2 and MBIP may promote each other's stability. Other ATAC subunits, such as GCN5, WDR5, and DR1, were not affected by *Atac2* or *Mbip* siRNA treatment (Fig. 2C, lanes 2 and 3). A similar effect was observed when ATAC2 was depleted in A549 and mouse C2C12 cells (Fig. 2D, lanes 2 and 6). In contrast to the case with ATAC2 and MBIP, GCN5 depletion had no effect on the stability of any tested ATAC or STAGA/TFTC subunits (Fig. 2C, lanes 1 and 4).

To evaluate the impact of decreased ATAC2 and MBIP levels on ATAC formation, we performed anti-WDR5 coim-

munoprecipitations, using extracts from cells treated with various siRNAs (Fig. 2C). While similar amounts of WDR5 were immunoprecipitated (Fig. 2C, lanes 5 to 8 in WDR5 blot), ATAC2 or MBIP depletion resulted in significantly decreased GCN5 and DR1 in the complex (Fig. 2C, lanes 6 and 7), suggesting that ATAC2 and MBIP are critical for ATAC integrity. In contrast, GCN5 depletion did not affect the coprecipitation of the tested ATAC subunits (Fig. 2C, lane 8). Coimmunoprecipitation experiments were also performed with an anti-GCN5 antibody (Fig. 2C, lanes 9 to 12), with similar findings consisting of decreased WDR5 and DR1 in the ATAC complex upon ATAC2 or MBIP depletion (lanes 10 and 11). However, the association of GCN5 with ADA2b and TAF12, two specific subunits of STAGA/TFTC, was not affected (Fig. 2C, lanes 10 and 11), supporting the notion that ATAC and STAGA/TFTC are distinct GCN5-containing complexes. As a control, GCN5 siRNA treatment led to decreased GCN5 as well as proportional reductions of other GCN5-associating proteins in ATAC and STAGA complexes (Fig. 2C, lane 12). The crucial role of ATAC2 in ATAC integrity was independently verified in A549 and mouse C2C12 cells (Fig. 2D, lanes 3, 4, 7, and 8). Taken together, our studies demonstrate that ATAC2 and MBIP stabilize each other and may function as a scaffold for the ATAC complex.

Loss of *Atac2* leads to reduced histone acetylation, cell death, and G_2/M arrest. Targeted disruption of *Drosophila Atac2* resulted in decreased H4 K16 acetylation without affecting the acetylation status of other lysines on histones H3 and H4 (49). We investigated whether a similar effect could be observed in A549 and HEK293 cells containing a doxycycline-inducible *Atac2* shRNA construct. A 6-day doxycycline treatment resulted in over 90% depletion of ATAC2 in both cell lines, as demonstrated by Western blotting analysis of ATAC2 immunoprecipitates (Fig. 3A, top panel). We compared the levels of acetylated histones under normal growth and doxycycline-induced conditions (Fig. 3A). The acetylation of H3 K9, H4 K5, H4 K12, and H4 K16 was reduced to at least 50% in the knockdown cells. However, no statistically significant changes were observed for residues H3 K14 and H4 K8 (Fig. 3A and B).

GCN5 plays an important role in cellular viability as well as in cell cycle progression. While disruption of mouse *Gcn5* leads to apoptosis of early embryonic cells (56), deletion of yeast *gcn5* results in accumulation of cells at G_2/M phase (62). Therefore, we examined the contribution of the ATAC complex to these important biological processes in A549 cells expressing *Atac2* shRNA. A 6-day doxycycline treatment resulted in double the apoptosis of A549 cells compared to that under normal growth conditions, as measured by a PI permeability assay (Fig. 3C). When we compared the cell cycle distribution of the viable population of control cells versus that of doxycycline-induced A549 cells, we found that while the percentage of cells in the S phase decreased from 40% to 29% after a 6-day doxycycline treatment, the number of cells in the G_2/M phase consistently increased from 6% to 14%, indicating a G_2/M arrest (Fig. 3D). Therefore, ATAC regulates both the cellular viability and cell cycle progression of A549 cells.

Targeted disruption of *Atac2* in mice leads to early embryonic lethality. *Gcn5* plays an essential role in mouse embryonic development. *Gcn5*-null mice fail to maintain dorsal mesoderm structures due to increased cell death and die at E10.5 (56). However, the respective contributions of STAGA/TFTC and ATAC to mouse development are not known. We generated an *Atac2* KO model to explore the potential role of the mammalian ATAC. Targeted disruption of mouse *Atac2* was achieved by a retroviral gene trap insertion located 313 bp downstream of exon 3 (Fig. 4A). Due to premature transcription termination, the mutant allele is expected to yield a 126-amino-acid polypeptide which lacks the majority of the primary sequence (779 amino acids), including the acetyltransferase domain. Mice carrying the mutant allele were generated successfully, as demonstrated by PCR-based screening of E8.5 embryos from heterozygotic crosses (Fig. 4B). While real-time reverse transcription-PCR detected the mRNA 5′ of the insertion cassette, likely corresponding to chimeric RNA molecules containing exons 1, 2, and 3 of *Atac2* and part of the insertion cassette, transcripts 3′ of exon 3 were absent in the mutant embryos, confirming that the insertion cassette interrupts *Atac2* transcription (data not shown). We also analyzed lysates from pooled E9.5 WT and homozygous mutant embryos by Western blotting (Fig. 4C). Antibodies directed to the C terminus of ATAC2 failed to detect any signal in the lanes corresponding to the two different pools of mutant embryonic extracts (Fig. 4C, lanes 3 and 4). No viable $Atac2^{-/-}$ mice survived to birth. Therefore, we screened several developmental stages to determine the timing of embryonic lethality. The ratio of $Atac2^{-/-}$ embryos was normal at E8.5 but lower than the expected Mendelian distribution at E9.5 to E10.5 (Table 2), suggesting that $Atac2^{-/-}$ embryos die at 8.5 to 11 days postconception. When we analyzed embryos at E7.5, $Atac2^{-/-}$ embryos were smaller than their $Atac2^{+/+}$ and $Atac2^{+/-}$ littermates, and this size difference was even more pronounced at E8.5 (Fig. 4D and E). Consistent with the requirement of ATAC for embryonic development, *Atac2* is expressed in multiple tissues, except for the developing heart, from E7.5 to E12.5 (Fig. 4F and data not shown).

Histological analyses confirmed the developmental delay; however, normal lineage allocation and differentiation were still evident (Fig. 5A). No obvious histological abnormalities were observed in extraembryonic tissues. Interestingly, many condensed and fragmented nuclei, which are features of apoptotic cells, were frequently observed in the $Atac2^{-/-}$ embryos (Fig. 5A). To confirm this, we performed immunohistochemical analysis of cleaved caspase-3, a marker for apoptosis. Very few apoptotic cells were present in $Atac2^{+/+}$ and $Atac2^{+/-}$ embryos, but apoptotic cells were markedly increased throughout the $Atac2^{-/-}$ embryos, especially in the densely packed neuroectoderm (Fig. 5B). Therefore, apoptosis appears to be an important contributing factor to the developmental delay. We next investigated the proliferative capacity of embryonic cells isolated from $Atac2^{-/-}$, $Atac2^{+/-}$, and $Atac2^{+/+}$ embryos by analyzing their cell cycle profiles with PI staining followed by FACS analysis. Consistent with the cleaved caspase-3 immunohistochemistry results, 10% of the cells from $Atac2^{-/-}$ embryos were present in the sub-G_1 fraction, as opposed to only 1% of cells derived from $Atac2^{+/+}$ embryos (Fig. 5C). In addition, cell cycle analysis revealed a 10% increase in the G_1 phase and a 12% decrease in the S phase, as well as a twofold increase in the G_2/M phase, for $Atac2^{-/-}$ cells (Fig. 5C and D). These results are similar to what we observed in cell lines and

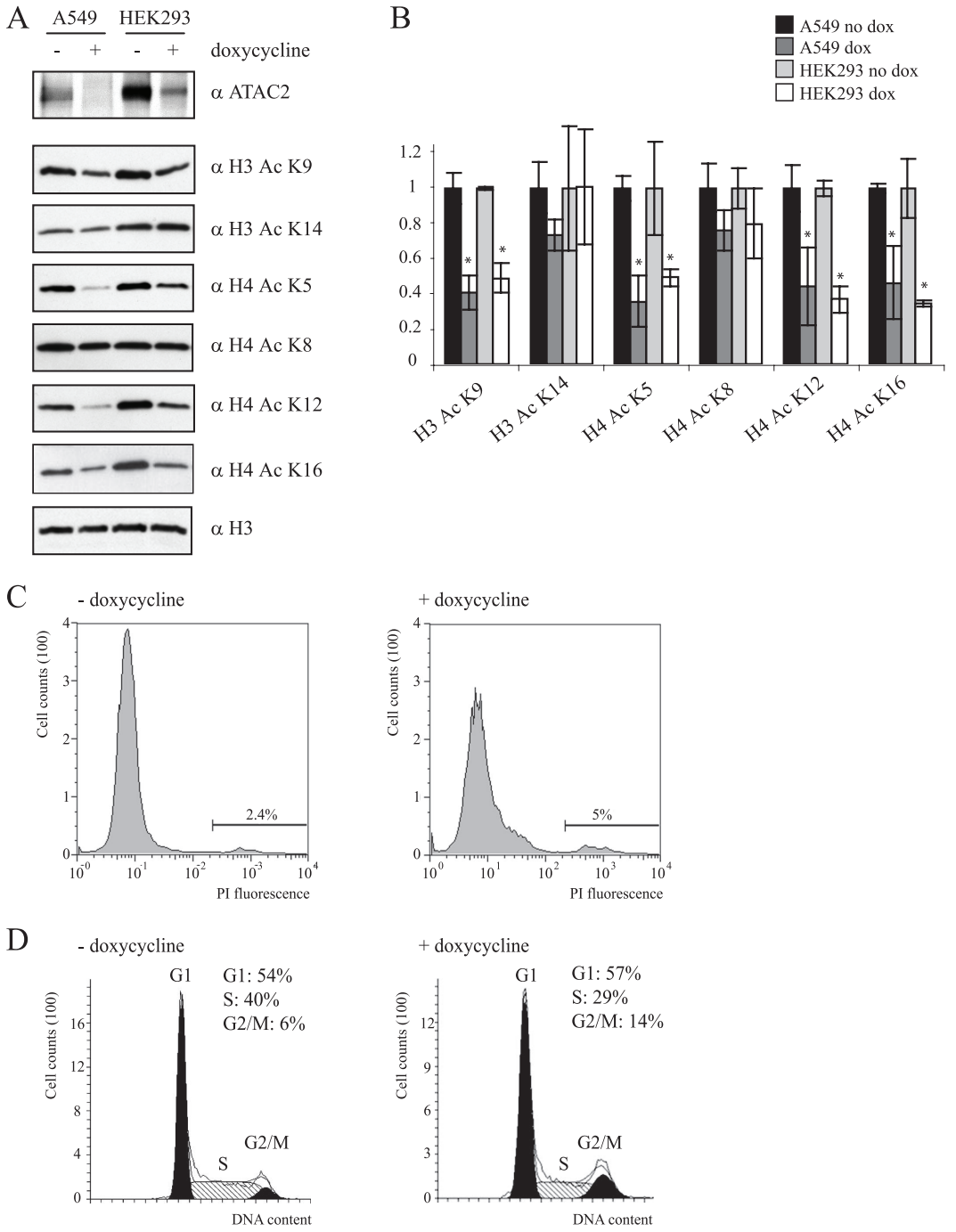

FIG. 3. Depletion of *Atac2* results in reduced levels of acetylated histones H3 and H4, cell death, and G_2/M arrest. (A) HEK293 and A549 stable cell lines expressing doxycycline-inducible *Atac2* shRNA were grown for 6 days in the absence or presence of doxycycline (− and + lanes, respectively). Whole-cell extracts were prepared and analyzed by anti-ATAC2 Western blotting of anti-ATAC2 immunoprecipitates (top panel). Alternatively, proteins were acid extracted and analyzed by Western blotting using antibodies against acetylated histones. (B) Quantification of the ratio of acetylated histone to histone H3 for A549 and HEK293 cells grown with and without doxycycline (dox) ($n = 3$). *P* values of <0.05 are shown with asterisks. (C and D) A549 cells carrying a doxycycline-inducible *Atac2* shRNA construct were grown for 6 days in the presence or absence of doxycycline. (C) Viability was measured by PI exclusion. The percentages represent cells that are positive for PI (dying and dead cells). (D) Cell cycle profiles were determined. A representative example of results from four independent experiments is shown.

confirm that ATAC2 is required for normal progression through the G_1 and G_2/M phases of the cell cycle.

Atac2 deficiency does not affect the expression of mesoderm and ectoderm markers. Mesoderm differentiation is abnormal in *Gcn5* mutant mice, particularly in paraxial mesoderm, chordamesoderm, and head mesoderm. These mice exhibit comparable expression of some mesoderm markers to that of their WT littermates at E7.5 to E8.0, but not thereafter (56). Al-

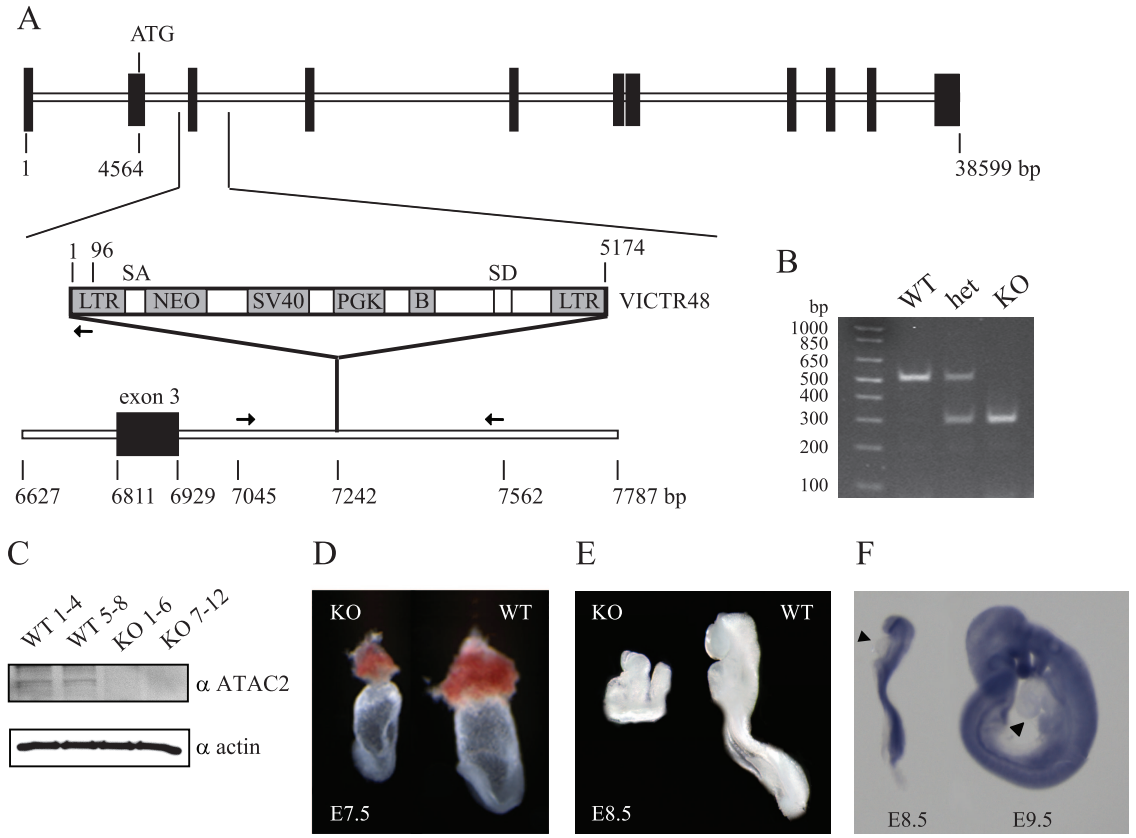

FIG. 4. Characterization of *Atac2*-deficient mice. (A) (Top) Schematic representation of the *Atac2* gene. Exons are displayed with black boxes. The position of the translation start codon (ATG) within exon 2 is shown. (Bottom) Magnification of the DNA region flanking exon 3, showing the position of the insertion cassette VICTR48 (not to scale). bp, base pairs; LTR, long terminal repeat; SA, splicing acceptor; NEO, neomycin resistance gene; SV40, simian virus 40 polyadenylation sequence A; PGK, phosphoglycerate kinase 1 promoter; B, Bruton's tyrosine kinase exon; SD, splice donor. Arrows indicate the positions of the three PCR primers used to genotype the different *Atac2* alleles. (B) Agarose gel displaying the three possible genotypes present in E8.5 embryos. A DNA ladder was loaded in the left lane. WT, homozygous WT; het, heterozygous; KO, homozygous KO. (C) Two different pools of lysates prepared from four WT (WT1-4 and WT5-8) and six KO (KO1-6 and KO7-12) embryos at E9.5 were analyzed by Western blotting, using antibodies against ATAC2 and actin. (D and E) Bright-field microscopy of WT and KO embryos at E7.5 and E8.5. (F) Whole-mount in situ hybridization using an *Atac2*-specific probe to stain WT E8.5 and E9.5 embryos. Arrowheads point to the position of the heart.

though no gross changes in the relative proportion of each tissue in cross sections were noted, we performed whole-mount in situ hybridization of mesoderm markers, including *Fgf8*, *Mlc2v*, *Tcf15*, *Dll*, and *Twist1*, to examine possible differences (Fig. 6). Similar to the case in *Gcn5* KO mice, expression of the primitive streak-enriched *Fgf8* gene was not altered in E8.5 *Atac2*$^{-/-}$ embryos (13, 56). The developing heart appeared to be unaffected in *Atac2*$^{-/-}$ embryos, as evidenced by a normal pattern of heart-specific *Mlc2v* staining (31). In contrast to *Gcn5* mutant embryos, marker expression in the paraxial mesoderm/somites (*Tcf15* and *Dll1*) (Fig. 6A and D), cranial mesoderm (*Twist*) (Fig. 6E), and notochord/floorplate (*Foxa2*) (Fig. 6H) was not significantly altered in the *Atac2*$^{-/-}$ embryos. However, unlike the WT embryos, the *Atac2*$^{-/-}$ KO mice lacked *Dll1* and *Wnt1* staining in the forebrain/midbrain (4) and dorsal spinal cord, respectively (Fig. 6A and F). This difference could be due to a generalized developmental delay and/or to increased apoptosis rather than a specific lineage defect, as these embryos were quite small and expression of *Fgf8* and *Pax3* was preserved in the neuroectoderm of the *Atac2* mutants (Fig. 6C and G). Taken together, these data show that *Atac2* deficiency does not appear to affect lineage specification and differentiation, but rather is required for the viability of partially differentiated cells.

TABLE 2. Genotype analysis of embryos from heterozygous intercrosses

Stage	Total no. of embryos	No. (%) of embryos			
		WT	Heterozygous	KO	Resorbed
E8.5	450	111 (25)	234 (52)	105 (23)	0
E9.5	70	18 (26)	38 (54)	9 (13)	5 (7)
E10.5	83	19 (23)	52 (62)	10 (12)	2 (2)
E11.5	51	16 (31)	28 (55)	0	7 (14)
E12.5	56	20 (36)	36 (65)	0	0

Destabilization of ATAC subunits in *Atac2* mutant mouse embryos. Our biochemical analysis of cell lines predicted the destabilization of selective ATAC subunits in the mouse embryo. We examined embryonic extracts from two different pools of WT and KO E9.5 embryos for steady-state levels of ATAC components. While *Atac2* deficiency did not affect

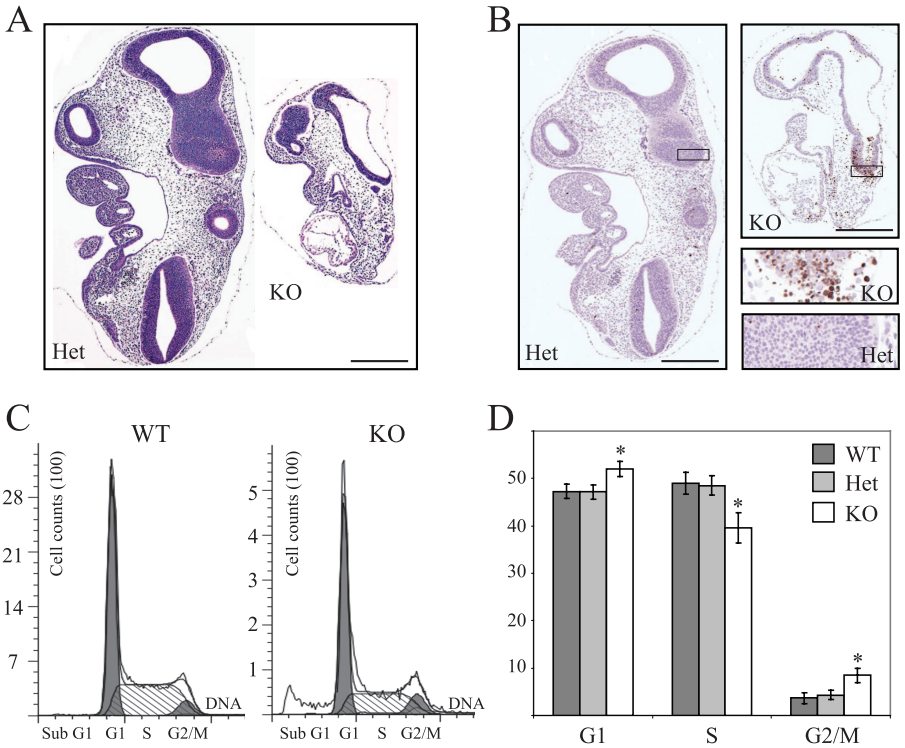

FIG. 5. *Atac2*-deficient embryos display increased apoptosis and G_2/M arrest. (A and B) Deciduae from E8.5 heterozygous and KO littermates were fixed and paraffin embedded, and sections were prepared and stained with hematoxylin and eosin (A) or antibodies against cleaved caspase-3 (B). Magnifications of the boxed areas are shown. Bars, 500 μm. (C and D) Cells from E9.5 WT, heterozygous (Het), and KO embryos were dissociated, fixed, and stained with PI, and DNA content was determined by FACS. (C) Representative cell cycle profiles from WT and KO samples are shown. (D) The percentages of cells in G_1, S, and G_2/M stages of the cell cycle are displayed for each genotype. Data shown are the means for at least three different embryos for each genotype. *P* values of <0.05 are indicated (*).

WDR5 and DR1, the levels of GCN5 and MBIP were significantly decreased (Fig. 7A), indicating that the stability of a subset of ATAC components was affected by the loss of ATAC2. As a specificity control, the levels of the STAGA/TFTC subunits ADA2b and TAF12 were unaltered in *Atac2*-deficient embryos (Fig. 7A). Comparing these results with our cell line data (Fig. 2C), it appears that the effects of ATAC2 depletion on GCN5 stability vary between mouse embryonic and cultured cells, suggesting that cellular context affects both the assembly and composition of GCN5-containing complexes and/or that the extent of ATAC2 depletion correlates with GCN5 stability.

We further examined the contribution of ATAC to embryonic histone acetylation by Western blotting (Fig. 7B). The amount of material isolated from E8.5 embryos limited the number of acetylated lysine residues that could be assayed from a single embryonic extract. While one set of six paired embryos was used for analyzing H3 K9, H3 K14, H4 K5, and H4 K12 acetylation, we used a different set for H4 K8 and H4 K16 acetylation. Acetylation levels were normalized to that of the histone H3 loading control for each embryo. Quantitative analysis showed that acetylation of H3 K9, H4 K5, H4 K12, and H4 K16 in the KO embryos was reduced to 40%, 50%, 50%, and 70% of WT levels, respectively (Fig. 7C). However, no statistically significant changes were observed for acetylated H3 K14 and H4 K8. The results from this experiment correlate with our observations from cell line analysis (Fig. 3A and B) and indicate that mouse and human ATAC have comparable substrate specificities.

DISCUSSION

We report the characterization of mammalian ATAC, a new GCN5-containing complex. ATAC and STAGA/TFTC share only three of their subunits, namely, GCN5, ADA3, and SGF29 (29, 42). Our studies demonstrate that ATAC is biochemically and functionally distinct from STAGA and TFTC. First, the MS analysis of affinity-purified ATAC did not reveal peptides for any TAFs or other STAGA/TFTC-specific proteins, such as ADA1/STAF42, SPT3, SPT7/STAF65γ, SAP130, USP22, and Ataxin-7 (23, 33, 63, 64). Second, we discovered novel proteins that were not previously identified as STAGA/TFTC subunits, such as ATAC2, DR1, MBIP, WDR5, YEATS2, and ZZZ3/ATAC1. Third, although both ATAC and STAGA/TFTC/dSAGA acetylate purified histones H3 and H4 in vitro, our results, combined with evidence from other labs, suggest that STAGA and TFTC target lysines on histone H3, while ATAC may preferentially target lysines on H4 tails, with some overlap on H3 K9. In *Drosophila* polytene chromosomes, mutations in *Ada2a* affect the levels of acetylated histone H4 on K5 and K12 but not the levels of acetylated H3 (12). In contrast, mutations in the *Drosophila* SAGA *Ada2b* or *Wda* gene affect the acetylation status of H3 K9 and K14 (22, 43, 45).

In addition to GCN5, vertebrates have another GCN5 *N*-

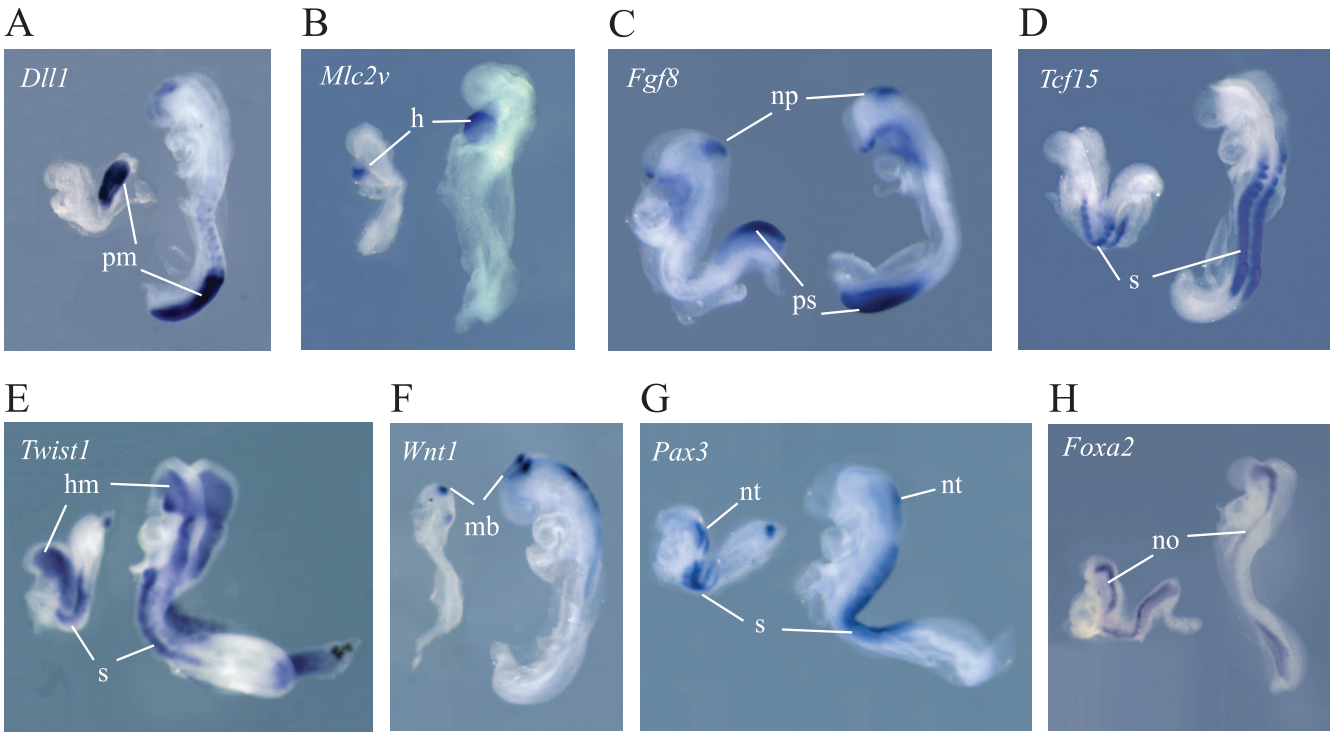

FIG. 6. Whole-mount in situ hybridization. The patterns of expression of the markers *Dll1*, *Mlc2v*, *Fgf8*, *Tcf15*, *Twist1*, *Wnt1*, *Pax3*, and *Foxa2* were determined for WT and *Atac2* KO E8.5 embryos. Lateral views of the embryos are shown. Mutant embryos are on the left side in each panel. h, developing heart; hm, head mesenchyme cells; mb, midbrain; no, notochord; np, neural plate; nt, neural tube; pm, presomitic mesoderm; ps, primitive streak; s, somites.

acetyltransferase family member, PCAF, which shares over 70% amino acid identity with GCN5 (36). PCAF is present in a multisubunit complex that contains many of the STAGA/TFTC subunits; however, the PCAF complex contains ADA2a (39). Our MS analysis of HEK293 cells expressing ATAC2-FLAG uncovered peptides for PCAF (data not shown), which raises the possibility that GCN5 and PCAF are interchangeable within the ATAC. Alternatively, ATAC2 and PCAF could form a distinct ATAC-like complex with novel subunits.

Workman and colleagues recently described novel subunits of the *Drosophila* ATAC (49). We identified nine proteins in mammalian ATAC that share sequence homology with dATAC subunits, including ATAC2, GCN5, ADA2a, ADA3, SGF29, WDR5, ZZZ3, DR1, and YEATS2. Besides these evolutionarily conserved subunits, there are some species-specific differences. None of our MS experiments yielded peptides for HCF-1, ERCC5, MOCS2, and GA repeat binding protein beta 2, the putative orthologues for *Drosophila* HCF, CHRAC14, CG10238, and ATAC3, respectively, suggesting that those proteins may be specific to dATAC (21, 49). In contrast, MBIP, a protein not conserved in flies, is unique to mammalian ATAC.

Independent of our studies, the Martinez laboratory described the purification of human ATAC from HeLa cells (52). Our purifications from ATAC2-FLAG and MBIP-FLAG HEK293 cells and mouse C2C12 cells confirm most of their MS results for FLAG-YEATS2 HeLa cells and also point out that ATAC is conserved in mammals. In addition, Martinez and colleagues demonstrated that the ATAC subunits YEATS2 and DR1 dimerize through their histone fold motifs to associate with TBP and repress basal transcription (52). In contrast, our three independent MS experiments did not identify UBAP2L, MAP3K7, POLE3, and POLE4 in human or mouse ATAC. Note that of all proteins identified in the FLAG-YEATS2 purification, those four proteins had the smallest numbers of peptides covered by the MS analysis (52), likely reflecting differences in the stringency of purification conditions and/or the proteins tagged for purification. Another difference likely attributed to experimental settings is the in vitro HAT activity of the human ATAC, which was reported to be specific for H3 (52). Our in vitro assay displayed activity on histones H3 and H4. Moreover, the in vivo analysis of histone acetylation in mouse embryonic extracts as well as human cell lines complements those results to demonstrate that mammalian ATAC targets specific lysine residues of histones H3 and H4.

Our work unveils a dual function for ATAC2. In addition to its catalytic activity on histone H4, ATAC2 provides architectural support with MBIP to promote ATAC stability. MBIP contains leucine zipper-like motifs predicted to form short amphipathic α-helixes, which could potentially associate with transcription factors to facilitate targeting of ATAC to specific chromatin regions (17). Another way to direct ATAC to active chromatin might involve WDR5, an ATAC subunit that has the capacity to bind methylated H3 K4 (55). Other components in ATAC might target nucleosomes. The SANT domain of c-Myb has been shown to bind histone H3 tails and position them for acetylation (35). Moreover, the SANT domains in

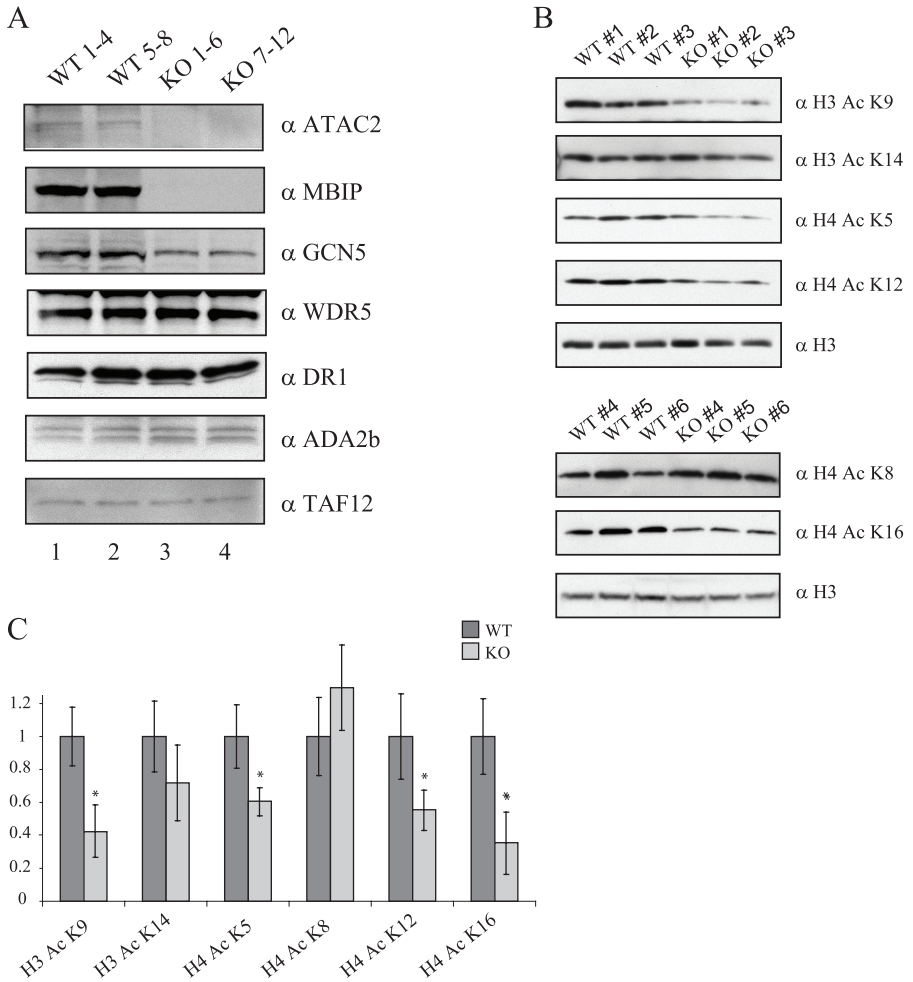

FIG. 7. Targeted disruption of *Atac2* leads to destabilization of MBIP and GCN5 and reduced histone acetylation (A) Two independent embryonic extracts from E9.5 WT (WT1-4 and WT5-8) and KO (KO1-6 and KO7-12) embryos were analyzed by Western blotting, using antibodies directed to ATAC and STAGA subunits. (B) Whole-cell extracts from six E8.5 WT embryos (WT #1 to WT #6) and six *Atac2* KO embryos (KO #1 to KO #6) were analyzed by Western blotting using antibodies against H3 ac K9, H3 ac K14, H4 ac K5, H4 ac K12, H4 ac K8, and H4 ac K16. Anti-H3 was used as a loading control. (C) Quantification of the amount of acetylated lysine normalized to the total H3 signal for WT and KO embryos ($n = 6$). *P* values of <0.05 are indicated (*).

ADA2a and ZZZ3/ATAC1 might enable the complex to associate with nucleosome tails in order to potentiate the catalytic activities of GCN5 and ATAC2, similar to what has been shown for the SANT domains in yeast Ada2 and Swi3 (5, 48).

We demonstrated that ATAC2 has a crucial role in stabilizing GCN5 and MBIP during embryonic development. Although sufficient embryonic material was not available to analyze the intactness of the ATAC in *Atac2*$^{-/-}$ embryos, our biochemical studies with cell lines suggest that ATAC is destabilized in *Atac2*$^{-/-}$ mutants. Compared to *Gcn5*$^{-/-}$ KO mice (56), *Atac2*-deficient embryos die at similar developmental stages, with likewise increased apoptosis in multiple lineages. However, *Atac2*$^{-/-}$ embryos did not display aberrations in the maintenance of markers for paraxial, axial, and cranial mesoderm at E8.5, as was observed in *Gcn5* KO mice. Thus, the less severe phenotypes of *Atac2* KO mice could be due to residual GCN5, which remains part of STAGA/TFTC during mesoderm development.

Although both fly and mouse *Atac2* mutants exhibit defects in histone acetylation, there are some intriguing differences between the two species. While *Atac2*-deficient fly embryos showed reduced levels of acetylation of H4 K16 (49), our mouse *Atac2* KO mice exhibited broader defects at multiple sites, including H4 K16, H4 K5, H4 K12, and H3 K9. Several factors could account for the observed differences. First, a PHD domain within residues 13 and 66 of *Drosophila* ATAC2 is absent from the mouse and human counterparts and may influence substrate selection. Second, the distinct subunit compositions of the complexes present in two different organisms could affect their substrate specificities. Third, Western blotting could be a more sensitive approach than whole-mount antibody staining, which allowed us to identify more subtle differences in acetylation patterns. The fact that H4 K16 is the residue where acetylation was decreased the most in our embryo analysis supports this idea. Nevertheless, histone acetylation defects might not be the only cause of embryonic lethality in *Atac2* mutant mice. The histone acetylation changes induced by ATAC2 depletion were similar in embryos and cell lines;

however, the cell lines exhibited a modest G_2/M arrest with only mildly increased apoptosis, in contrast to the mutant embryos, which showed massive apoptosis. Therefore, it is conceivable that ATAC may have additional substrates, such as proteins involved in the regulation of apoptosis, particularly in developing embryonic cells. Our future efforts will be directed at understanding how GCN5 is targeted to various complexes, how each complex distinguishes among potential substrates, and how these complexes facilitate progression through embryonic development.

ACKNOWLEDGMENTS

We thank the following members of the Genentech core facilities: Nicole Kahoud, Sheila Bheddah, Jian Jiang, Julio Ramirez, Laszlo Komuves, Jeffrey Eastham-Anderson, Laurie Gilmour, Krista Bowman, and Alberto Estevez. We also thank Weilan Ye's group for initial analysis of *Atac2* expression in mouse embryos and John Lowe and Kevin Leong for critical readings of the manuscript.

The KO mice were produced in a collaboration between Genentech and Lexicon Pharmaceuticals (The Woodlands, TX) to analyze the functions of about 500 secreted and transmembrane proteins.

REFERENCES

1. **Abmayr, S. M., T. Yao, T. Parmely, and J. L. Workman.** 2006. Preparation of nuclear and cytoplasmic extracts from mammalian cells. Curr. Protoc. Mol. Biol. **12:**12.1.
2. **Balasubramanian, R., M. G. Pray-Grant, W. Selleck, P. A. Grant, and S. Tan.** 2002. Role of the Ada2 and Ada3 transcriptional coactivators in histone acetylation. J. Biol. Chem. **277:**7989–7995.
3. **Banerjee, B., D. Bhattacharya, and G. V. Shivashankar.** 2006. Chromatin structure exhibits spatio-temporal heterogeneity within the cell nucleus. Biophys. J. **91:**2297–2303.
4. **Bettenhausen, B., M. Hrabe de Angelis, D. Simon, J. L. Guenet, and A. Gossler.** 1995. Transient and restricted expression during mouse embryogenesis of Dll1, a murine gene closely related to Drosophila Delta. Development **121:**2407–2418.
5. **Boyer, L. A., M. R. Langer, K. A. Crowley, S. Tan, J. M. Denu, and C. L. Peterson.** 2002. Essential role for the SANT domain in the functioning of multiple chromatin remodeling enzymes. Mol. Cell **10:**935–942.
6. **Brand, M., J. G. Moggs, M. Oulad-Abdelghani, F. Lejeune, F. J. Dilworth, J. Stevenin, G. Almouzni, and L. Tora.** 2001. UV-damaged DNA-binding protein in the TFTC complex links DNA damage recognition to nucleosome acetylation. EMBO J. **20:**3187–3196.
7. **Brand, M., K. Yamamoto, A. Staub, and L. Tora.** 1999. Identification of TATA-binding protein-free TAFII-containing complex subunits suggests a role in nucleosome acetylation and signal transduction. J. Biol. Chem. **274:**18285–18289.
8. **Brownell, J. E., J. Zhou, T. Ranalli, R. Kobayashi, D. G. Edmondson, S. Y. Roth, and C. D. Allis.** 1996. Tetrahymena histone acetyltransferase A: a homolog to yeast Gcn5p linking histone acetylation to gene activation. Cell **84:**843–851.
9. **Candau, R., P. A. Moore, L. Wang, N. Barlev, C. Y. Ying, C. A. Rosen, and S. L. Berger.** 1996. Identification of human proteins functionally conserved with the yeast putative adaptors ADA2 and GCN5. Mol. Cell. Biol. **16:**593–602.
10. **Carre, C., D. Szymczak, J. Pidoux, and C. Antoniewski.** 2005. The histone H3 acetylase dGcn5 is a key player in *Drosophila melanogaster* metamorphosis. Mol. Cell. Biol. **25:**8228–8238.
11. **Cavusoglu, N., M. Brand, L. Tora, and A. Van Dorsselaer.** 2003. Novel subunits of the TATA binding protein free TAFII-containing transcription complex identified by matrix-assisted laser desorption/ionization-time of flight mass spectrometry following one-dimensional gel electrophoresis. Proteomics **3:**217–223.
12. **Ciurciu, A., O. Komonyi, T. Pankotai, and I. M. Boros.** 2006. The *Drosophila* histone acetyltransferase Gcn5 and transcriptional adaptor Ada2a are involved in nucleosomal histone H4 acetylation. Mol. Cell. Biol. **26:**9413–9423.
13. **Crossley, P. H., and G. R. Martin.** 1995. The mouse Fgf8 gene encodes a family of polypeptides and is expressed in regions that direct outgrowth and patterning in the developing embryo. Development **121:**439–451.
14. **Dou, Y., T. A. Milne, A. J. Tackett, E. R. Smith, A. Fukuda, J. Wysocka, C. D. Allis, B. T. Chait, J. L. Hess, and R. G. Roeder.** 2005. Physical association and coordinate function of the H3 K4 methyltransferase MLL1 and the H4 K16 acetyltransferase MOF. Cell **121:**873–885.
15. **Doyon, Y., W. Selleck, W. S. Lane, S. Tan, and J. Cote.** 2004. Structural and functional conservation of the NuA4 histone acetyltransferase complex from yeast to humans. Mol. Cell. Biol. **24:**1884–1896.
16. **Eberharter, A., S. John, P. A. Grant, R. T. Utley, and J. L. Workman.** 1998. Identification and analysis of yeast nucleosomal histone acetyltransferase complexes. Methods **15:**315–321.
17. **Fukuyama, K., M. Yoshida, A. Yamashita, T. Deyama, M. Baba, A. Suzuki, H. Mohri, Z. Ikezawa, H. Nakajima, S. Hirai, and S. Ohno.** 2000. MAPK upstream kinase (MUK)-binding inhibitory protein, a negative regulator of MUK/dual leucine zipper-bearing kinase/leucine zipper protein kinase. J. Biol. Chem. **275:**21247–21254.
18. **Goppelt, A., G. Stelzer, F. Lottspeich, and M. Meisterernst.** 1996. A mechanism for repression of class II gene transcription through specific binding of NC2 to TBP-promoter complexes via heterodimeric histone fold domains. EMBO J. **15:**3105–3116.
19. **Grant, P. A., A. Eberharter, S. John, R. G. Cook, B. M. Turner, and J. L. Workman.** 1999. Expanded lysine acetylation specificity of Gcn5 in native complexes. J. Biol. Chem. **274:**5895–5900.
20. **Gray, D. C., K. P. Hoeflich, L. Peng, Z. Gu, A. Gogineni, L. J. Murray, M. Eby, N. Kljavin, S. Seshagiri, M. J. Cole, and D. P. Davis.** 2007. pHUSH: a single vector system for conditional gene expression. BMC Biotechnol. **7:**61.
21. **Guelman, S., T. Suganuma, L. Florens, S. K. Swanson, C. L. Kiesecker, T. Kusch, S. Anderson, J. R. Yates III, M. P. Washburn, S. M. Abmayr, and J. L. Workman.** 2006. Host cell factor and an uncharacterized SANT domain protein are stable components of ATAC, a novel dAda2A/dGcn5-containing histone acetyltransferase complex in *Drosophila*. Mol. Cell. Biol. **26:**871–882.
22. **Guelman, S., T. Suganuma, L. Florens, V. Weake, S. K. Swanson, M. P. Washburn, S. M. Abmayr, and J. L. Workman.** 2006. The essential gene *wda* encodes a WD40 repeat subunit of *Drosophila* SAGA required for histone H3 acetylation. Mol. Cell. Biol. **26:**7178–7189.
23. **Helmlinger, D., S. Hardy, S. Sasorith, F. Klein, F. Robert, C. Weber, L. Miguet, N. Potier, A. Van-Dorsselaer, J. M. Wurtz, J. L. Mandel, L. Tora, and D. Devys.** 2004. Ataxin-7 is a subunit of GCN5 histone acetyltransferase-containing complexes. Hum. Mol. Genet. **13:**1257–1265.
24. **Inostroza, J. A., F. H. Mermelstein, I. Ha, W. S. Lane, and D. Reinberg.** 1992. Dr1, a TATA-binding protein-associated phosphoprotein and inhibitor of class II gene transcription. Cell **70:**477–489.
25. **Kikuchi, H., Y. Takami, and T. Nakayama.** 2005. GCN5: a supervisor in all-inclusive control of vertebrate cell cycle progression through transcription regulation of various cell cycle-related genes. Gene **347:**83–97.
26. **Kouzarides, T.** 2007. Chromatin modifications and their function. Cell **128:**693–705.
27. **Kraus, V. B., J. A. Inostroza, K. Yeung, D. Reinberg, and J. R. Nevins.** 1994. Interaction of the Dr1 inhibitory factor with the TATA binding protein is disrupted by adenovirus E1A. Proc. Natl. Acad. Sci. USA **91:**6279–6282.
28. **Kuo, M. H., J. Zhou, P. Jambeck, M. E. Churchill, and C. D. Allis.** 1998. Histone acetyltransferase activity of yeast Gcn5p is required for the activation of target genes in vivo. Genes Dev. **12:**627–639.
29. **Kurabe, N., K. Katagiri, Y. Komiya, R. Ito, A. Sugiyama, Y. Kawasaki, and F. Tashiro.** 2007. Deregulated expression of a novel component of TFTC/STAGA histone acetyltransferase complexes, rat SGF29, in hepatocellular carcinoma: possible implication for the oncogenic potential of c-Myc. Oncogene **26:**5626–5634.
30. **Liu, X., M. Vorontchikhina, Y. L. Wang, F. Faiola, and E. Martinez.** 2008. STAGA recruits Mediator to the Myc oncoprotein to stimulate transcription and cell proliferation. Mol. Cell. Biol. **28:**108–121.
31. **Lyons, I., L. M. Parsons, L. Hartley, R. Li, J. E. Andrews, L. Robb, and R. P. Harvey.** 1995. Myogenic and morphogenetic defects in the heart tubes of murine embryos lacking the homeo box gene Nkx2-5. Genes Dev. **9:**1654–1666.
32. **Martinez, E., T. K. Kundu, J. Fu, and R. G. Roeder.** 1998. A human SPT3-TAFII31-GCN5-L acetylase complex distinct from transcription factor IID. J. Biol. Chem. **273:**23781–23785.
33. **Martinez, E., V. B. Palhan, A. Tjernberg, E. S. Lymar, A. M. Gamper, T. K. Kundu, B. T. Chait, and R. G. Roeder.** 2001. Human STAGA complex is a chromatin-acetylating transcription coactivator that interacts with pre-mRNA splicing and DNA damage-binding factors in vivo. Mol. Cell. Biol. **21:**6782–6795.
34. **Mermelstein, F., K. Yeung, J. Cao, J. A. Inostroza, H. Erdjument-Bromage, K. Eagelson, D. Landsman, P. Levitt, P. Tempst, and D. Reinberg.** 1996. Requirement of a corepressor for Dr1-mediated repression of transcription. Genes Dev. **10:**1033–1048.
35. **Mo, X., E. Kowenz-Leutz, Y. Laumonnier, H. Xu, and A. Leutz.** 2005. Histone H3 tail positioning and acetylation by the c-Myb but not the v-Myb DNA-binding SANT domain. Genes Dev. **19:**2447–2457.
36. **Nagy, Z., and L. Tora.** 2007. Distinct GCN5/PCAF-containing complexes function as co-activators and are involved in transcription factor and global histone acetylation. Oncogene **26:**5341–5357.
37. **Neuwald, A. F., and D. Landsman.** 1997. GCN5-related histone *N*-acetyltransferases belong to a diverse superfamily that includes the yeast SPT10 protein. Trends Biochem. Sci. **22:**154–155.
38. **Nie, Z., Z. Yan, E. H. Chen, S. Sechi, C. Ling, S. Zhou, Y. Xue, D. Yang, D. Murray, E. Kanakubo, M. L. Cleary, and W. Wang.** 2003. Novel SWI/SNF chromatin-remodeling complexes contain a mixed-lineage leukemia chromosomal translocation partner. Mol. Cell. Biol. **23:**2942–2952.

39. **Ogryzko, V. V., T. Kotani, X. Zhang, R. L. Schlitz, T. Howard, X.-J. Yang, B. H. Howard, J. Qin, and Y. Nakatani.** 1998. Histone-like TAFs within the PCAF histone acetylase complex. Cell **94:**35–44.
40. **Ornaghi, P., P. Ballario, A. M. Lena, A. Gonzalez, and P. Filetici.** 1999. The bromodomain of Gcn5p interacts in vitro with specific residues in the N terminus of histone H4. J. Mol. Biol. **287:**1–7.
41. **Owen, D. J., P. Ornaghi, J. C. Yang, N. Lowe, P. R. Evans, P. Ballario, D. Neuhaus, P. Filetici, and A. A. Travers.** 2000. The structural basis for the recognition of acetylated histone H4 by the bromodomain of histone acetyltransferase gcn5p. EMBO J. **19:**6141–6149.
42. **Palhan, V. B., S. Chen, G. H. Peng, A. Tjernberg, A. M. Gamper, Y. Fan, B. T. Chait, A. R. La Spada, and R. G. Roeder.** 2005. Polyglutamine-expanded ataxin-7 inhibits STAGA histone acetyltransferase activity to produce retinal degeneration. Proc. Natl. Acad. Sci. USA **102:**8472–8477.
43. **Pankotai, T., O. Komonyi, L. Bodai, Z. Ujfaludi, S. Muratoglu, A. Ciurciu, L. Tora, J. Szabad, and I. Boros.** 2005. The homologous *Drosophila* transcriptional adaptors ADA2a and ADA2b are both required for normal development but have different functions. Mol. Cell. Biol. **25:**8215–8227.
44. **Peth, A., C. Berndt, W. Henke, and W. Dubiel.** 2007. Downregulation of COP9 signalosome subunits differentially affects the CSN complex and target protein stability. BMC Biochem. **8:**27.
45. **Qi, D., J. Larsson, and M. Mannervik.** 2004. *Drosophila* Ada2b is required for viability and normal histone H3 acetylation. Mol. Cell. Biol. **24:**8080–8089.
46. **Shia, W. J., S. Osada, L. Florens, S. K. Swanson, M. P. Washburn, and J. L. Workman.** 2005. Characterization of the yeast trimeric-SAS acetyltransferase complex. J. Biol. Chem. **280:**11987–11994.
47. **Solloway, M. J., and E. J. Robertson.** 1999. Early embryonic lethality in Bmp5;Bmp7 double mutant mice suggests functional redundancy within the 60A subgroup. Development **126:**1753–1768.
48. **Sterner, D. E., X. Wang, M. H. Bloom, G. M. Simon, and S. L. Berger.** 2002. The SANT domain of Ada2 is required for normal acetylation of histones by the yeast SAGA complex. J. Biol. Chem. **277:**8178–8186.
49. **Suganuma, T., J. L. Gutierrez, B. Li, L. Florens, S. K. Swanson, M. P. Washburn, S. M. Abmayr, and J. L. Workman.** 2008. ATAC is a double histone acetyltransferase complex that stimulates nucleosome sliding. Nat. Struct. Mol. Biol. **15:**364–372.
50. **Wang, G. G., C. D. Allis, and P. Chi.** 2007. Chromatin remodeling and cancer. II. ATP-dependent chromatin remodeling. Trends Mol. Med. **13:**373–380.
51. **Wang, L., C. Mizzen, C. Ying, R. Candau, N. Barlev, J. Brownell, C. D. Allis, and S. L. Berger.** 1997. Histone acetyltransferase activity is conserved between yeast and human GCN5 and is required for complementation of growth and transcriptional activation. Mol. Cell. Biol. **17:**519–527.
52. **Wang, Y. L., F. Faiola, M. Xu, S. Pan, and E. Martinez.** 2008. Human ATAC is a GCN5/PCAF-containing acetylase complex with a novel NC2-like histone fold module that interacts with the TATA-binding protein. J. Biol. Chem. **283:**33808–33815.
53. **Weiskirchen, R., and A. M. Gressner.** 2000. The cysteine- and glycine-rich LIM domain protein CRP2 specifically interacts with a novel human protein (CRP2BP). Biochem. Biophys. Res. Commun. **274:**655–663.
54. **White, R. J., B. C. Khoo, J. A. Inostroza, D. Reinberg, and S. P. Jackson.** 1994. Differential regulation of RNA polymerases I, II, and III by the TBP-binding repressor Dr1. Science **266:**448–450.
55. **Wysocka, J., T. Swigut, T. A. Milne, Y. Dou, X. Zhang, A. L. Burlingame, R. G. Roeder, A. H. Brivanlou, and C. D. Allis.** 2005. WDR5 associates with histone H3 methylated at K4 and is essential for H3 K4 methylation and vertebrate development. Cell **121:**859–872.
56. **Xu, W., D. G. Edmondson, Y. A. Evrard, M. Wakamiya, R. R. Behringer, and S. Y. Roth.** 2000. Loss of Gcn5l2 leads to increased apoptosis and mesodermal defects during mouse development. Nat. Genet. **26:**229–232.
57. **Yeung, K. C., J. A. Inostroza, F. H. Mermelstein, C. Kannabiran, and D. Reinberg.** 1994. Structure-function analysis of the TBP-binding protein Dr1 reveals a mechanism for repression of class II gene transcription. Genes Dev. **8:**2097–2109.
58. **Yokoyama, A., Z. Wang, J. Wysocka, M. Sanyal, D. J. Aufiero, I. Kitabayashi, W. Herr, and M. L. Cleary.** 2004. Leukemia proto-oncoprotein MLL forms a SET1-like histone methyltransferase complex with menin to regulate Hox gene expression. Mol. Cell. Biol. **24:**5639–5649.
59. **Zambrowicz, B. P., A. Abuin, R. Ramirez-Solis, L. J. Richter, J. Piggott, H. Beltran del Rio, E. C. Buxton, J. Edwards, R. A. Finch, C. J. Friddle, A. Gupta, G. Hansen, Y. Hu, W. Huang, C. Jaing, B. W. Key, Jr., P. Kipp, B. Kohlhauff, Z. Q. Ma, D. Markesich, R. Payne, D. G. Potter, N. Qian, J. Shaw, J. Schrick, Z. Z. Shi, M. J. Sparks, I. Van Sligtenhorst, P. Vogel, W. Walke, N. Xu, Q. Zhu, C. Person, and A. T. Sands.** 2003. Wnk1 kinase deficiency lowers blood pressure in mice: a gene-trap screen to identify potential targets for therapeutic intervention. Proc. Natl. Acad. Sci. USA **100:**14109–14114.
60. **Zambrowicz, B. P., G. A. Friedrich, E. C. Buxton, S. L. Lilleberg, C. Person, and A. T. Sands.** 1998. Disruption and sequence identification of 2,000 genes in mouse embryonic stem cells. Nature **392:**608–611.
61. **Zhang, H., D. O. Richardson, D. N. Roberts, R. Utley, H. Erdjument-Bromage, P. Tempst, J. Cote, and B. R. Cairns.** 2004. The Yaf9 component of the SWR1 and NuA4 complexes is required for proper gene expression, histone H4 acetylation, and Htz1 replacement near telomeres. Mol. Cell. Biol. **24:**9424–9436.
62. **Zhang, W., J. R. Bone, D. G. Edmondson, B. M. Turner, and S. Y. Roth.** 1998. Essential and redundant functions of histone acetylation revealed by mutation of target lysines and loss of the Gcn5p acetyltransferase. EMBO J. **17:**3155–3167.
63. **Zhang, X. Y., M. Varthi, S. M. Sykes, C. Phillips, C. Warzecha, W. Zhu, A. Wyce, A. W. Thorne, S. L. Berger, and S. B. McMahon.** 2008. The putative cancer stem cell marker USP22 is a subunit of the human SAGA complex required for activated transcription and cell-cycle progression. Mol. Cell **29:**102–111.
64. **Zhao, Y., G. Lang, S. Ito, J. Bonnet, E. Metzger, S. Sawatsubashi, E. Suzuki, X. Le Guezennec, H. G. Stunnenberg, A. Krasnov, S. G. Georgieva, R. Schule, K. Takeyama, S. Kato, L. Tora, and D. Devys.** 2008. A TFTC/STAGA module mediates histone H2A and H2B deubiquitination, coactivates nuclear receptors, and counteracts heterochromatin silencing. Mol. Cell **29:**92–101.